This is the peer reviewed author accepted manuscript (post print) version of a published work that appeared in final form in:

Asamoah, Richmond K, Zanin, Massimiliano, Gascooke, Jason, Skinner, William & Addai-Mensah, Jonas 2019 'Refractory gold ores and concentrates part 1: mineralogical and physico-chemical characteristics', Mineral processing and extractive metallurgy: transactions of the institute of mining and metallurgy online, pp. 10-13

This un-copyedited output may not exactly replicate the final published authoritative version for which the publisher owns copyright. It is not the copy of record. This output may be used for non-commercial purposes.

The final definitive published version (version of record) is available at: https://doi.org/10.1080/25726641.2019.1626659

Persistent link to the Research Outputs Repository record:
http://researchoutputs.unisa.edu.au/11541.2/138364

General Rights
Copyright and moral rights for the publications made accessible in the Research Outputs Repository are retained by the authors and/or other copyright owners and it is a condition of accessing publications that users recognize and abide by the legal requirements associated with these rights.

- Users may download and print one copy for the purpose of private study or research.
- You may not further distribute the material or use it for any profit-making activity or commercial gain
- You may freely distribute the persistent link identifying the publication in the Research Outputs Repository

If you believe that this document breaches copyright please contact us providing details, and we will remove access to the work immediately and investigate your claim.

Refractory Gold Ores and Concentrates Part 1: Mineralogical and Physico-Chemical Characteristics

Richmond K. Asamoah[1], Massimiliano Zanin[1], Jason Gascooke[2], William Skinner[1], Jonas Addai-Mensah[*1,3]

[1]Future Industries Institute, University of South Australia, Mawson Lakes, SA 5095, Australia

[2]College of Science and Engineering, Flinders University, Bedford Park, Australia

[3]Department of Mining and Process Engineering, Namibia University of Mines and Technology, Windhoek, Namibia

[*]Corresponding Author: jonas.addai-mensah@unisa.edu.au

Abstract

A comprehensive mineralogical and physico-chemical examination of two refractory gold ores and concentrates from the Ghanaian gold province was conducted to gain a better understanding of the differences in performance of gold cyanidation. Both ore were mainly silicates, carbonates, oxide, phosphate and sulphides. Flotation of the ground ores produced concentrates with noticeable differences. Whilst both mainly contained sulphides and silicates, apatite was present in one flotation concentrate and dolomite in the other. Bio-oxidation of the apatite-bearing concentrate produced jarosite-bearing bio-oxidised product. Bio-oxidation of the dolomite-bearing concentrate yielded a jarosite-free bio-oxidised product with lower bassanite content but higher gypsum, graphitic carbon, and preg-robbing effect compared with the jarosite-bearing bio-oxidised product. The jarosite minerals appeared to aid gangue mineral agglomeration and also encapsulated auriferous minerals which attenuated the bio-oxidation process and reduced gold extraction.

Key words:

Refractory gold ores; flotation and bio-oxidised gold ores; ore mineralogy and chemistry; jarosite formation; process control and automation.

1. Introduction

Increase in demand for efficacious gold (Au) extraction methods is underpinned by several ore-inherent properties. These include the rapid decline in gold ore grades, the increase in the ore mineralogical and chemical complexity, and the intractable nature of minerals to treatment technologies (Lunt and Weeks, 2016).

Gold ore mineralogy is defined by geogenic activities and may be used to predict the ores' refractoriness (Yannopoulos, 1991). The rapid depletion of high grade ores coupled with the occurrence of complex ore mineralogy, in recent years, warrant improvement of hydrometallurgical techniques which are capable of extracting low grade ores profitably. To date, limited knowledge exists on the mineralogical and physico-chemical changes in complex gold ores at different hydrometallurgical treatment stages. Under standard physico-chemical leaching conditions, gold ores that yield < 90 wt.% Au are known as refractory ores (Table 1). These refractory ores (Figure 1) pose major mine productivity challenges given their less predictive and complex associations, yet are the ores of future mines (Deschênes, 2016).

To render refractory gold ores susceptible to cyanidation, various pre-treatment methods [e.g., roasting and biological oxidation (BIOX®)] have been integrated into extraction process flowsheets, depending upon the type of refractoriness (Ellis, 2003; Miller et al., 2016). Bio-oxidation treatment, using Chemolithotrophic bacteria, liberates gold from the refractory sulphide mineral matrix (e.g., arsenopyrite and pyrite). It has found wide applications due to the high abundance of sulphide minerals, benign operating conditions, and lower capital (CAPEX) and operational (OPEX) expenditures, especially for relatively small operations (Miller and Brown, 2016).

Three well-known intractable challenges persist in the application of the bio-oxidation technique. These include the formation of cyanide consuming and gold passivating

intermediate sulphide species (e.g., elemental sulphur), requirement of significant amount of alkali (e.g., lime) to modify acidic product (pH ~ 1.8) for cyanidation, and the inability to prevent gold preg-robbing by ore-inherent carbonaceous matter.

A typical gold extraction process route used for treating the refractory gold ore is schematically shown in Figure 2. There is limited published information on the effect of ore mineralogy and physico-chemical characteristics on gold extraction performance across unit operations. This paper presents a comprehensive physico-chemical and mineralogical examination on two refractory gold ores and concentrates from the Ghanaian gold province, previously noted to contain organogenic carbonaceous matter (Abotsi and Osseo-Asare, 1986; Guay, 1981).

2. Materials and methods

2.1 Ore and sample preparation

Approximately 10 kg each of two, typical comminuted run-of-mine (ROM) ores, and their corresponding flotation concentrates and bio-oxidised products (5 kg each) were sampled from gold processing plant (due to a confidentiality agreement, the name of the processing plant that supplied the samples cannot be disclosed). The sampling points are coloured “bold” in Figure 2. One ROM ore type has been reported to produce bio-oxidised product which yields higher gold recovery (≈ 90 wt.%) compared with the other ore type (≈ 70 wt.%). The higher gold yielding ROM ore, flotation concentrate and bio-oxidised product are referred to as ROM1, FC1 and BP1, respectively. Similarly, the lower gold yielding ROM ore, flotation concentrate and bio-oxidised product are referred to as ROM2, FC2 and BP2. ROM1 is getting depleted from the deposit, and being replaced by the ROM2 to maintain production.

2.2 Sample Characterisation

2.2.1 Ore mineralogy and microscopic investigations

Semi-quantitative X-ray diffraction (QXRD) analysis of the samples was performed using Scintag ARL X'tra diffractometer equipped with XPowder and SIROQUANT^{TM} V3 for mineral identification and quantification, respectively. Quantitative evaluation of minerals by scanning electron microscopy (QEMSCAN) was further performed on the flotation concentrates and bio-oxidation products. Further microscopic study of the samples included use of scanning electron microscopy (SEM) (Camscan CFSE CS44, Cambridge, UK) coupled with energy dispersive X-ray spectroscopy (EDXS).

2.2.2 Bulk and surface chemistry

Complete bulk and surface chemical characterisation were achieved using X-ray fluorescence spectrometry (XRF)/laser ablation mass spectroscopy and ethylenediamine tetra acetic acid disodium salt (EDTA) extraction, respectively. Loss on ignition (LOI) was determined using thermogravimetric analyser. The gold head grade was also determined by fire assay whilst solution speciation was achieved by inductive coupled plasma – atomic emission spectrometry (ICP-AES).

2.2.3 Sulphur and carbon speciation

The total sulphur content was determined by total combustion using a carbon/sulphur analyser. Sulphate-sulphur and elemental sulphur were determined by spectroscopic and gravimetric techniques, respectively. Also, carbon speciation was determined at 1400°C by three-stage analysis comprising determination of total carbon, non-carbonate carbon and graphitic carbon, deploying required specific pre-treatment.

2.2.4 Preg-robbing effect of carbon

For assessing the preg-robbing nature of carbonaceous matter (PEC), 10 g of the higher (BP1) and lower (BP2) gold yielding bio-oxidised products were contacted with 0.04 dm^3 of 20 mg/dm^3 gold solution and agitated at 200 rpm on a Ratek Orbital Mixer Incubator for 24 h, using the procedure of Ofori-Sarpong et al. (2010). The preg-robbing effect (g Au/t con) was determined using Eq.1.

$$\mathrm{PEC} = \mathrm{V} \times [\mathrm{IC} - (\mathrm{FC} - \mathrm{CE})] \cdot \left(\frac{1}{\mathrm{WC}}\right) \qquad \textbf{Eq. 1}$$

where IC and FC are initial and final gold concentrations in solution, CE represents control gold concentration in solution, WC is sample weight, and V is volume of gold solution used.

2.2.5 Carbon Structural Analysis

Raman microspectroscopy was used to characterise the graphitic carbon *in situ* using polished sections. This analysis was determined for the two bio-oxidised products, commercial activated carbon from Chemquest and highly oriented pyrolytic graphite (HOPG, ZYH grade, Coherent Scientific) for comparison. The Raman spectra were collected with a confocal Raman microscope (XplorRA Horiba Scientific) using an excitation wavelength of 638 nm and a 50X objective (numerical aperture 0.6). Individual spectra at locations on the sample were recorded with a 30 s integration time and repeated 6 times to generate an averaged spectrum.

2.2.6 Particle size distribution and surface area

The particle size analysis was carried out by laser diffraction (Mastersizer 2000, Malvern Instruments Ltd., UK). Measurements were done in de-ionised water at room temperature, with 5 min ultrasonication. The specific surface area of mineral particles were determined by a 5-point N_2 adsorption Brunauer-Emmett-Teller (BET) method using Quantachrome Quadrawin

BET analyser (Quantachrome Instruments, USA). All analyses were replicated three times and mean value reported herein.

3. Results and discussion

3.1 Mineralogical characteristics

The mineralogical characteristics of the six samples are shown in Figure 3 and Table 2. The major mineralogical differences between the two ore types (Clinozoisite-ROM1, Siderite-ROM2), flotation concentrates (Dolomite-FC1, Apatite-FC2) and bio-oxidised products (Jarosite-BP2 only) are evidently shown in Figure 3 alongside varying proportions of other silicates, oxides, sulphides, phosphates and carbonates. The data revealed presence of higher oxide and silicate minerals, and lower sulphide flotation recovery in sample FC2 compared with sample FC1. The lower auriferous minerals content in sample FC2 is consistent with the lower gold grade revealed in the next section. The observed secondary sulphate minerals were produced during and/or after bio-oxidation of the concentrates.

To further confirm the QXRD data, a more detailed mineralogical investigation using QEMSCAN was conducted. Generally, the percent composition of other trace mineral phases identified by QEMSCAN analysis were consistent and within statistical error margin of the QXRD data (± 1 – 3%). The QEMSCAN data also showed smaller grain sizes for pyrite and arsenopyrite in samples FC2 and BP2 than samples FC1 and BP1 which confirms greater occurrence composite mineral in the former (Table 2). Linking the flotation concentrates to the ROM ores, it can be concluded that, ROM1 and ROM2 are two different ores, characterised by different mineralogy and grain size, within the same deposit. The fine grain nature of the minerals in ROM2 could impact the flotation grade-recovery curve, leading to lower auriferous sulphide recovery.

Pyrite bio-oxidation reaction is given in Eq. 2. Besides sulphide oxidation, other minerals phases such as dolomite, apatite and larnite leach during bio-oxidation due to the high acidic condition deployed. These leached species encourage different pulp chemistries and interactions. For instance, for every 1 t of FC2 bio-oxidised, about 38 kg of apatite is leached. This consequently leaves about 7.3 kg phosphorus in solution. Although phosphorus is used by the bacteria as nutrient source, the amount introduced by the sample FC2 is about 8.1 times greater than the required BIOMIN amounts (0.9 kg/t). Since little attention is paid to these process stream variabilities, routine addition of phosphorus is further carried out at the bio-oxidation conditioning stage (Figure 2) and hence resulting in a total of 8.2 kg/t (9.1 times greater than the required amounts) phosphorus pulp concentration. More ore mineralogy-linked process control and automation could mitigate this challenge.

$$2FeS_2 + 7\tfrac{1}{2}O_2 + H_2O \rightleftharpoons H_2SO_4 + Fe_2(SO_4)_3 \qquad \textbf{Eq. 2}$$

The Ca-based minerals consumed (dolomite and apatite) encouraged formation of new Ca-rich compounds (bassanite and gypsum), respectively, in the bio-oxidised products. Some previous studies (Dutrizac and Chen, 2010) have also shown that phosphate ions, in our case leached from sample FC2, facilitate co-precipitation of jarosite and calcium sulphates at the typical bio-oxidation pH range (1.0 – 1.8) (Eqs. 3 – 7). They showed that at very high phosphate concentrations, only phosphate-bearing sodium jarosites are formed, thereby suggesting that the presence of jarosites in BP2 is due to the presence of leachable apatite in FC2. Calcium from lime neutralisation and dolomite may also contribute to the secondary calcium sulphate mineral formation. Such subtle mineralogical and physico-chemical differences can define a successful operation.

$$3H_2SO_4 + Ca_3(PO_4)_2 \rightleftharpoons 3CaSO_4 + 2H_3PO_4 \qquad \textbf{Eq. 3}$$

$$CaSO_4 + 2H_2O \rightleftharpoons CaSO_4.2H_2O \qquad \textbf{Eq. 4}$$

$$CaSO_4 + 0.5H_2O \rightleftharpoons CaSO_4.0.5H_2O \quad \textbf{Eq. 5}$$

$$3Fe^{3+} + K^+ + 2SO_4^{2-} + 6H_2O \rightleftharpoons KFe_3(SO_4)_2(OH)_6 + 6H^+ \quad \textbf{Eq. 6}$$

$$3Fe^{3+} + 2K^+ + PO_4^{3-} + SO_4^{2-} + 6H_2O \rightleftharpoons K_2Fe_3PO_4SO_4(OH)_6 + 6H^+ \quad \textbf{Eq. 7}$$

3.2 Bulk chemistry

The results from the bulk chemical analysis are presented in Table 3. Since Au is the metal of interest, changes in its grade through the various units operations is interesting. It was evident that, the ore (ROM2) yielding lower gold recoverable bio-oxidised product had lesser gold head grade (1.3 g/t) compared with the depleting ore (ROM1; 2.8 g/t). The higher gold grade in FC1 compared with FC2 is consistent with the higher sulphide content of the former relative to the latter. However, based on the extent of increase in gold grade after flotation, the dilution of gold-bearing minerals by gangue minerals was greater in sample FC2 than in sample FC1. This is also consistent with the lower gold grade ore (ROM2), finer grain size and hence poor liberation.

3.3 Sulphur/carbon speciation and preg-robbing characteristics

Table 4 shows the speciation of sulphur in the ores, flotation concentrates and bio-oxidised products which were consistent with the mineralogical and bulk chemical data. The evidently greater sulphide-sulphur content in sample BP2 compared with sample BP1 agrees with the higher amount of pyrite, pyrrhotite and chalcopyrite present in the former. The poor gold recovery in sample BP2 compared with sample BP1 could also be ascribed to the poor sulphide-sulphur oxidation. Furthermore, the poor sulphide-sulphur oxidation agrees with encapsulation

of sulphide minerals by secondary minerals or the poor liberation of sulphide minerals due to their fine grained associations.

Table 5 shows the speciation of carbon in the samples, and the preg-robbing effect of carbonaceous matter in samples BP1 and BP2. The non-carbonate carbon which comprise both graphitic carbon and organic carbon (humic acid-like) are capable of adsorbing dissolved gold from cyanide solution (Abotsi and Osseo-Asare, 1986; Guay, 1981; Miller and Brown, 2016). The preg-robbing strength of the non-carbonate carbon species, characterised by the preg-robbing value (PRV), were further investigated. The results showed that the preg-robbing values of both samples BP1 and BP2 are statistically the same. It was evident that, the increase in preg-robbing effect for sample BP1 is due to its greater graphitic carbon content. The PRV for BP1 and BP2 could, however, be misleading as the influence of organic carbon is not considered. Raman spectroscopy of non-carbonate carbon in BP1 and BP2 can be used to determine the difference in the preg-robbing ability (Helm et al., 2009). Following spectra deconvolution (Figure 4), sample BP2 yielded a Raman Ratio of 0.8 whilst sample BP1 yielded 1.1, confirming the PRV results.

3.4 Surface chemistry

Percent chemical species extracted by EDTA relative to the bulk, for the flotation concentrates and bio-oxidised products, are presented in Table 6. The investigated chemical species were selected based on the mineralogical/chemical difference of the investigated samples. The results show that, copper, arsenic, iron, and sulphur were sparingly affected by EDTA in sample FC1 and FC2 because majority of the elements existed as sulphides. Very small oxidized species of copper, arsenic, iron and sulphur occurred at the surfaces of the sulphide minerals in the flotation concentrates. The increase in concentration of EDTA extractable As, Ca, Cu, Fe, and S after BIOX® agrees with the formation of oxidation products. Significant

leaching of the chemical species were observed in sample BP1 prior to the introduction of EDTA, revealing the refractoriness of the secondary minerals associated with sample BP2. This could be due to the jarosite mineral which was only present in sample BP2. The leaching difficulty displayed by gypsum and bassanite in the bio-oxidised product suggests their complex association with refractory jarosite minerals. Gold particles, encapsulated by surface refractory sulphate minerals, will be unavailable for cyanidation. The result also suggests that, the poor sulphide-sulphur oxidation is due to the refractoriness of passivating species (jarosite) in sample BP2.

3.5 Mineral associations

Figure 5 shows the discrete gold-gangue mineral associations in the flotation concentrates and bio-oxidised product, determined using QEMSCAN-TMS. The higher gold-pyrite association in sample BP1 compared to BP2 suggests galvanic interactions which may improve gold extraction whilst gold leaching attenuation by the greater gold-chalcopyrite content occur in sample BP2 compared with BP1 (Aghamirian and Yen, 2005). These complex associations, including gold-jarosite association, will inspire different individual impacts on the overall gold extraction. There is a need to establish the amount of gold associated with each group of mineral.

Backscattered electron (BSE/SEM) photomicrographs of FC1 and FC2 are shown in Figure 6. The observed finely disseminated gold particles is consistent with the above data. Association of the minerals in the bio-oxidised products is very important for diagnosing their impact on gold extraction. BSE photomicrographs of the bio-oxidised product yielding lower gold recovery (BP2) are shown in Figure 7. It was evident that, most of the unreacted sulphide minerals were surface coated by the secondary sulphate minerals (jarosite and gypsum; Figure C1). Whether or not the absence of these secondary sulphate minerals on the surfaces of the

large pyrite minerals will enhance their bio-oxidation is not clear, given the well-known sparingly soluble nature of pyrites during bio-oxidation compared with arsenopyrites (Miller and Brown, 2016).

In addition, encapsulation of the sulphide minerals by sulphate or oxide mineral phases (Figure 7D) could either help or hinder processing. For instance, coating of auriferous sulphides attenuates the liberation of encapsulated gold particles. The coatings may also be eliminated by mechanical shear force during cyanidation and thereby exhibiting deleterious impact (e.g., high reagent consumption, galvanic interactions, etc.) on gold extraction rate and yield. Furthermore, cementation of coagulated particles on auriferous pyrite by jarosite was observed and could account for the poor sulphide-sulphur oxidation in BP2 compared with BP1 (Figures 7E and F).

Closer examination of the secondary minerals (e.g., gypsum and jarosite) and gangue agglomerate surfaces revealed association of jarosite with gypsum and other aluminosilicate agglomerates (Figure 8). The occurrence of jarosite grains in gypsum suggest passivation effect of jarosite on gypsum. This is a significant difference between the secondary mineral associations in the two bio-oxidised samples and serves as good indication of the refractoriness posed by jarosite on the extraction process. The observation also confirms the EDTA extraction data. The result further showed that jarosite minerals formed solid bridges between gangue mineral agglomerates (Figures 8C), consistent with previous studies by Sadowski (1999). The specific role of each of the variable cause of refractoriness in BP2 is further investigated in the Part 2 of this work (Asamoah et al., 2019).

Figure 9 shows the BSE photomicrographs of minerals in sample BP1 where both etched sulphides (Figure 9 A) and oxidic polymorphs of sulphide minerals (Figure 9B and C) were also found. The oxidation of the sulphide minerals followed an order: the “easiest-to-leach” to

the “difficult-to-leach” minerals, being made evident by the faster leaching of gudmundite (FeSbS, Figure 9A) from associated arsenopyrite and pyrite (Figure 9C). It is worth noting that, unlike sample BP2, gangue mineral agglomerates were not observed in sample BP1. Hence, the formation of refractory jarosite minerals, agglomeration of value and gangue minerals, and passivation of gold-bearing minerals by jarosite could be a major contributor to low gold extraction in sample BP2 than in sample BP1 (Figure 10).

3.6 Particle size distribution and specific surface area

The samples are polydispersed with samples FC1 and FC2 displaying statistically the same particle size density distribution (Figure 11A). However, sample FC1 yielded finer particles whilst sample FC2 yielded coarser particles following bio-oxidation. The increase in particle size for sample BP2 is consistent with the crystallization of secondary minerals which passivate and cement gangue minerals agglomerates. The BET specific surface area of the flotation concentrates and bio-oxidised products are shown in Figure 11B. The observed specific surface areas of samples BP1 and BP2 are consistent with their respective particle size distribution results. The result suggests that, the passivation and/or gangue mineral agglomerate cementation by jarosite minerals did not only increase the particle size but also blocked fissures or pores.

Knowledge of these ore variabilities are vital in controlling existing unit operations in an efficacious manner and/or designing new techniques, considering the changing chemical properties. Establishing ways of preventing refractory secondary sulphate mineral formation through fundamental studies will be useful in designing appropriate process control tools (Asamoah et al., 2018a; Asamoah et al., 2018b). Part 2 of this research focuses on the mineralisation and deportment of gold in the flotation concentrates and bio-oxidised products,

providing information on the quantitative amount of gold associated with each refractory causing class.

4. Conclusions

A Comprehensive mineralogical and physico-chemical examination on two refractory gold ores (ROM1 and ROM2), flotation concentrates (FC1 and FC2), and bio-oxidised products (BP1 and BP2) from the Ghanaian gold province have been conducted. One ore type (ROM2) produces lower gold yielding bio-oxidised products (BP2) whilst the other ore type (ROM1) produces higher gold yielding bio-oxidised product (BP1). More importantly, the ore yielding higher gold recovery is being depleted, leaving the ore which yields lower gold recovery product. From the results, the following conclusions can be made.

1. Although the two mined ores originated from same deposit, they showed marked differences in mineralogical characteristics. The mineralogical differences (e.g., mineral abundance, association, grain size) of the processed ore defined the response of each sub-processes of the operation. This confirms the noted variable gold recovery from the two bio-oxidised products generated from the two ore types.
2. Bio-oxidation of the flotation concentrate (FC2) which contained apatite produced jarosite which attenuated the oxidation process and enhanced gangue mineral agglomeration. This product also showed a markedly lower specific surface area due to surface passivation and blocking of fissures. On the other hand, bio-oxidation of the flotation concentrate (FC1) which contained dolomite did not produce jarosite. However, it produced lower bassanite concentration and increased gypsum concentration.

3. EDTA surface extraction results confirmed the surface passivation action of the sulphate minerals which agrees hand-in-hand with the ore bulk chemistry and mineralogy. Furthermore, carbonaceous matter in the two bio-oxidised products showed equal preg-robbing strength. Notwithstanding, higher preg-robbing effect was noted for the higher gold yielding product (BP1) compared with the lower gold yielding product (BP2), owing to the greater graphitic carbon content of the former.

Acknowledgement

Financial support from the Research Training Program (RTP) of the Australian Government is gratefully appreciated. The Australian National Fabrication Facility (ANFF) is acknowledged for providing access to the Raman microscope used in this study. We are grateful to the reviewers for their input.

References

Abotsi, G.M. and Osseo-Asare, K., 1986. Surface chemistry of carbonaceous gold ores I. Characterization of the carbonaceous matter and adsorption behavior in aurocyanide solution. International Journal of Mineral Processing, 18(3): 217-236.

Afidenyo, J.K., 2008. Microbial pre-treatment of double refractory gold ores, Queen's University, Kingston, Ontario, Canada, 179 pp.

Aghamirian, M.M. and Yen, W.T., 2005. Mechanisms of galvanic interactions between gold and sulfide minerals in cyanide solution. Minerals Engineering, 18(4): 393-407.

Asamoah, R.K., Amankwah, R.K. and Addai-Mensah, J., 2014. Cyanidation of Refractory Gold Ores: A Review, 3rd UMaT Biennial International Mining and Mineral Conference. University of Mines and Technology, Tarkwa, Ghana.

Asamoah, R.K., Skinner, W. and Addai-Mensah, J., 2018a. Alkaline cyanide leaching of refractory gold flotation concentrates and bio-oxidised products: The effect of process variables. Hydrometallurgy, 179: 79-93.

Asamoah, R.K., Skinner, W. and Addai-Mensah, J., 2018b. Leaching behaviour of mechano-chemically activated bio-oxidised refractory flotation gold concentrates. Powder Technology, 331: 258-269.

Asamoah, R.K., Zanin, M., Skinner, W. and Addai-Mensah, J., 2019. Refractory Gold Ores and Concentrates Part 2: Gold Mineralisation and Deportment in Flotation Concentrates and Bio-oxidised Products. Mineral Processing and Extractive Metallurgy, (Under Review).

Chen, J., Li, Y. and Zhao, C., 2014. First principles study of the occurrence of gold in pyrite. Computational Materials Science, 88(0): 1-6.
Deschênes, G., 2016. Advances in the cyanidation of gold. In: M.D. Adam (Ed.), Gold Ore Processing - Project Development and Operations. Elsevier, Amsterdam, Netherlands, pp. 429-445.
Dutrizac, J.E. and Chen, T.T., 2010. The behaviour of phosphate during jarosite precipitation. Hydrometallurgy, 102(1): 55-65.
Ellis, S., 2003. Ultra fine grinding - A practical alternative to oxidative treatment of refractory gold ores, Eighth Mill Operators Conference. One Mine, Townsville, QLD, pp. 11 - 17.
Guay, W.J., 1981. The treatment of refractory gold ores containing carbonaceous material and sulfides. In: W.j. Schlitt, W.C. Larson and J.B. Hiskey (Eds.), Gold and Silver: Leaching, Recovery and Economics. American Institute of Mining, Metallurgical, and Petroleum Engineers, Inc., New Jersey, USA, pp. 17-22.
Helm, M., Vaughan, J., Staunton, W. and Avraamides, J., 2009. An investigation of the carbonaceous component of preg-robbing gold ores, World gold conference 2009. The Southern African Institute of Mining and Metallurgy, pp. 139-144.
Lunt, D. and Weeks, T., 2016. Process flowsheet selection. In: M.D. Adams (Ed.), Gold Ore Processing - Project Development and Operations. Elsevier, Amsterdam, Netherlands, pp. 113-129.
Miller, J.D., Wan, R.-Y. and Díaz, X., 2016. Preg-robbing gold ores. In: M.D. Adams (Ed.), Gold Ore Processing: Project Development and Operations. Elsevier, Amsterdam, Netherlands, pp. 885 - 907.
Miller, P. and Brown, A.R.G., 2016. Bacterial oxidation of refractory gold concentrates. In: M.D. Adams (Ed.), Gold Ore Processing - Project Development and Operations. Elsevier, Amsterdam, Netherlands, pp. 359 - 372.
Ofori-Sarpong, G., Tien, M. and Osseo-Asare, K., 2010. Myco-hydrometallurgy: Coal model for potential reduction of preg-robbing capacity of carbonaceous gold ores using the fungus, Phanerochaete chrysosporium. Hydrometallurgy, 102(1): 66-72.
Sadowski, Z., 1999. Adhesion of microorganism cells and jarosite particles on the mineral surface. In: R. Amils and A. Ballester (Eds.), Process Metallurgy. Elsevier, Madrid, Spain, pp. 393-398.
Yannopoulos, J.C., 1991. The extractive metallurgy of gold. Van Nostrand Reinhold, New York, USA, 281 pp.

List of Figures

Figure 1

Schematic diagram of: (A) physically locked gold in gangue mineral; (B) chemically locked gold in pyrite interstitial lattice site (Asamoah et al., 2014; Chen et al., 2014). Not drawn to scale.

Figure 2

Flowsheet for processing refractory gold ore (sulphidic gold ores). Sample points are shown in "bold".

Figure 3

Semi-quantitative XRD of the comminuted run of mine ores, flotation concentrates, and bio-oxidised products.

Figure 4

Raman spectra of HOPG, carbonaceous matter in the bio-oxidised products and activated carbon.

Figure 5

Discrete gold-gangue mineral association in the flotation concentrates and bio-oxidised products using TMS mode of QEMSCAN.

Figure 6

BSE/SEM photomicrographs showing the complex mineral associations in the flotation concentrates yielding lower (FC2- A) and higher (FC1- B) gold recoveries.

Figure 7

BSE/SEM photomicrographs of the bio-oxidised product yielding lower gold recovery.

Figure 8

BSE/SEM photomicrographs showing jarosite-gypsum (A and B), and jarosite-aluminosilicate-agglomerate (C) associations in the bio-oxidised product yielding lower gold recovery.

Figure 9

BSE/SEM photomicrographs of the bio-oxidised product yielding higher gold recovery.

Figure 10

Schematic diagram of the jarosite formation effect on gangue minerals and gold particles in the lower gold yielding bio-oxidised product (BP2).

Figure 11

(A) Particle size distribution; and (B) Specific surface area of the flotation concentrates, and bio-oxidised products.

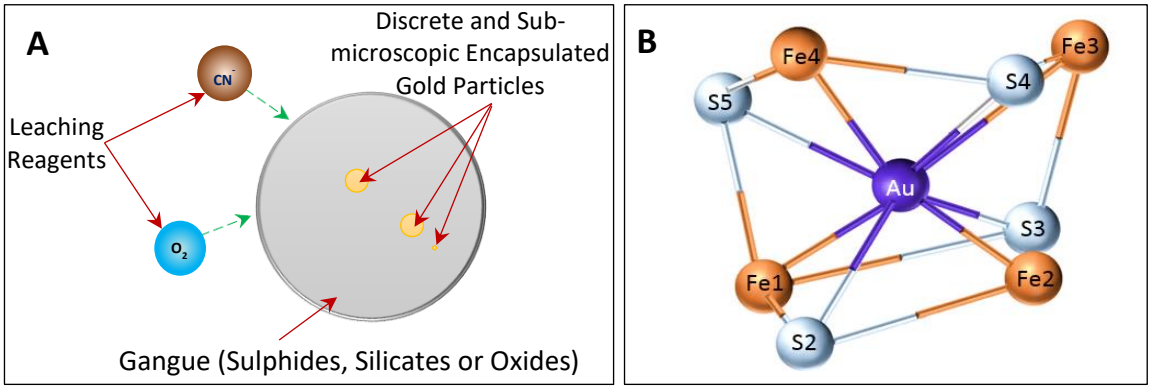
A
Discrete and Sub-microscopic Encapsulated Gold Particles
Leaching Reagents
CN⁻
O₂
Gangue (Sulphides, Silicates or Oxides)
B
Fe4
Fe3
S5
S4
Au
S3
Fe1
Fe2
S2

Figure 1. Schematic diagram of: (A) physically locked gold in gangue mineral; (B) chemically locked gold in pyrite interstitial lattice site (Asamoah et al., 2014; Chen et al., 2014). Not drawn to scale.

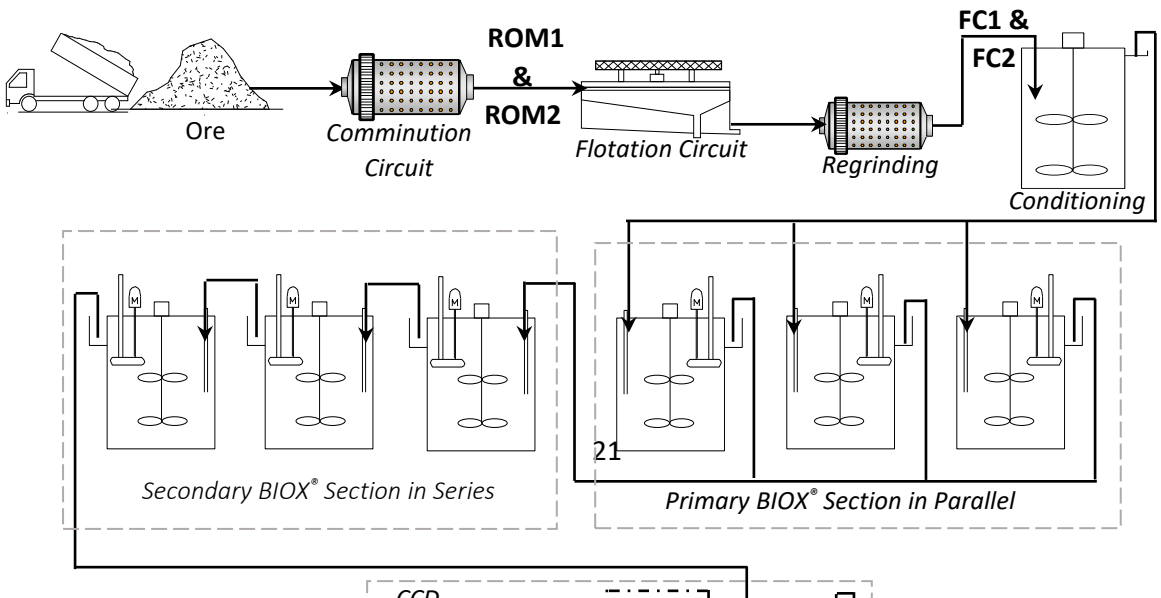

Figure 2. Flowsheet for processing refractory gold ore (sulphidic gold ores). Sample points are shown in “bold”.

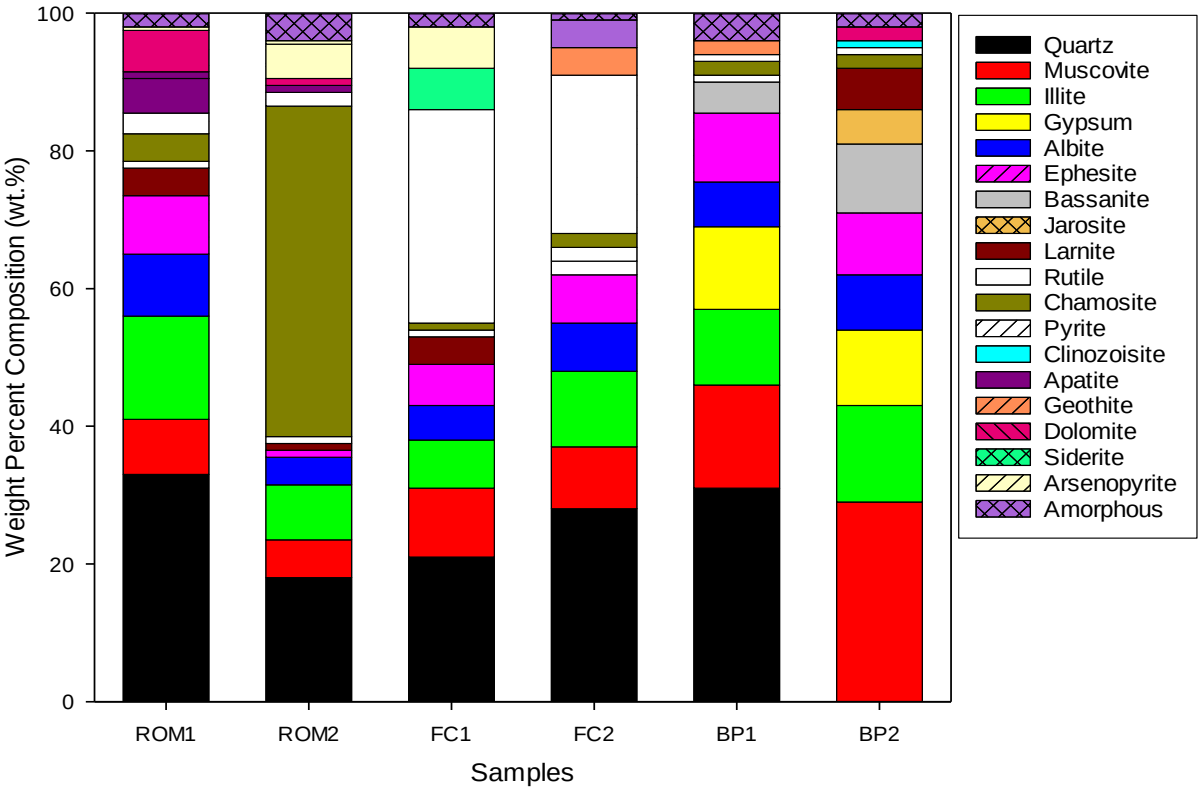

Figure 3. Semi-quantitative XRD of the comminuted run of mine ores, flotation concentrates, and bio-oxidised products.

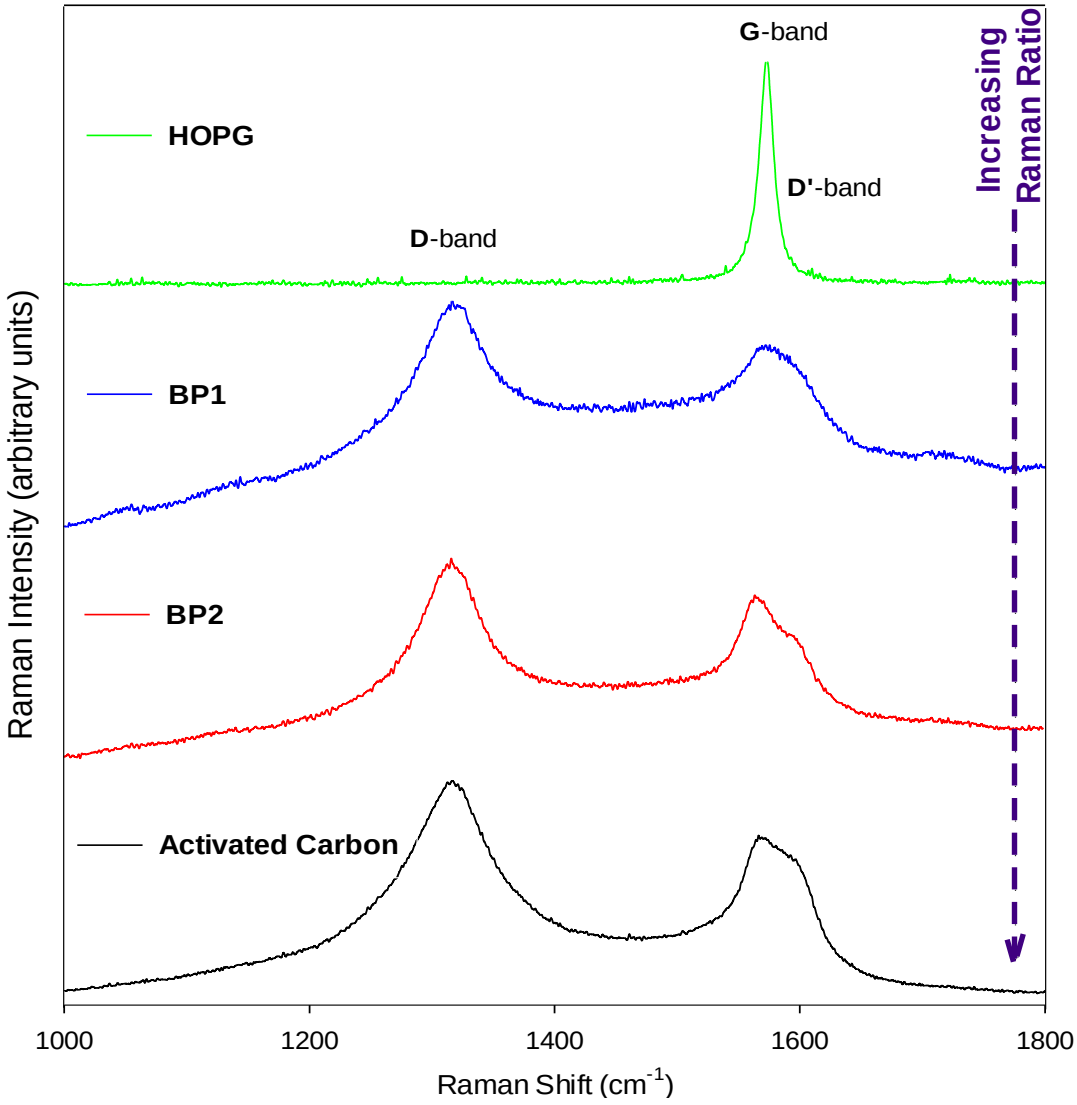

Figure 4. Raman spectra of HOPG, carbonaceous matter in the bio-oxidised products and activated carbon.

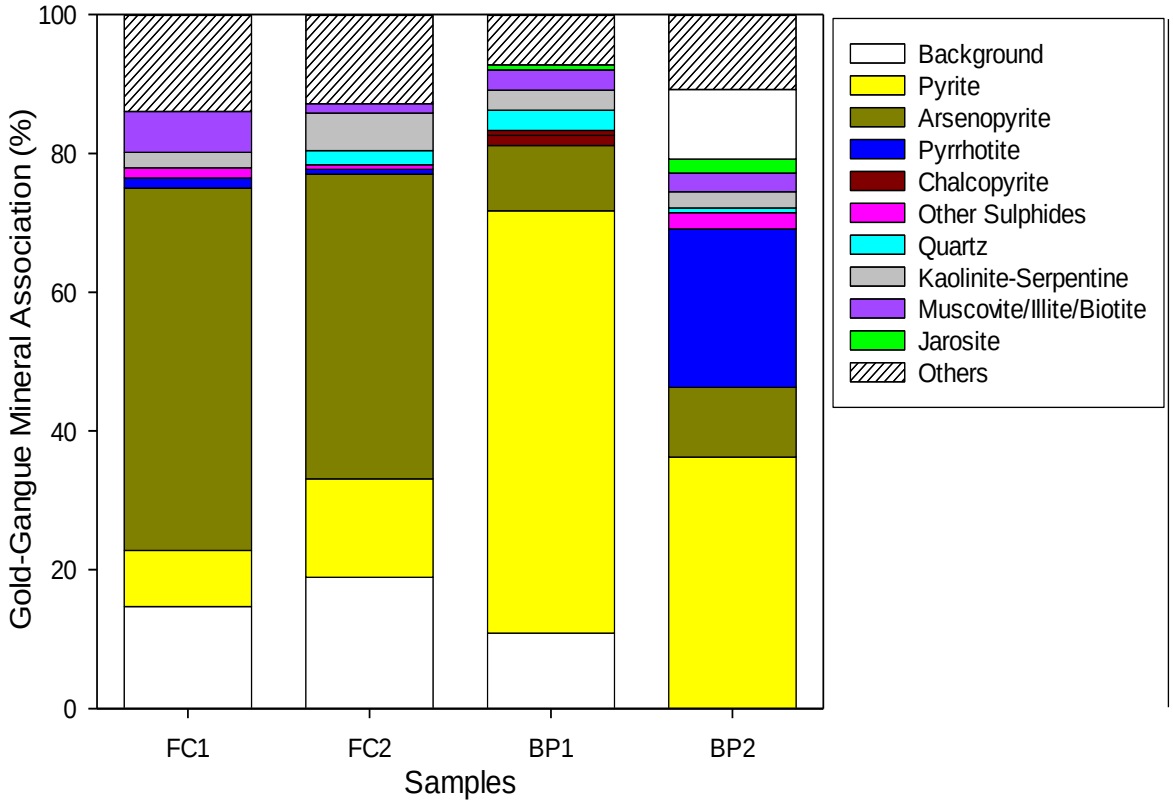

Figure 5. Discrete gold-gangue mineral association in the flotation concentrates and bio-oxidised products using TMS mode of QEMSCAN.

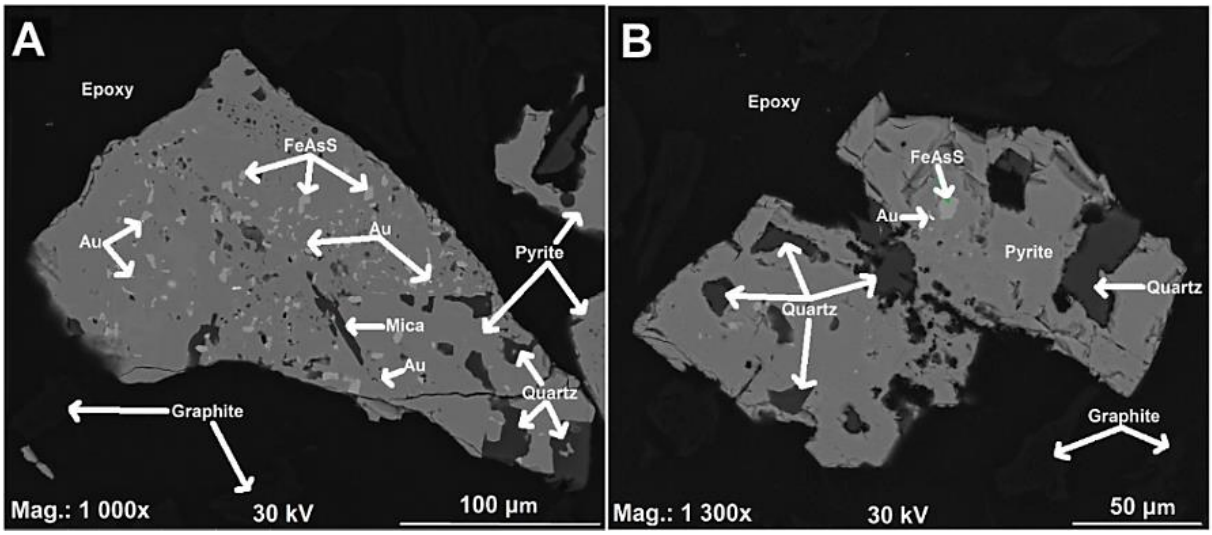

Figure 6. BSE/SEM photomicrographs showing the complex mineral associations in the flotation concentrates yielding lower (FC2- A) and higher (FC1- B) gold recoveries

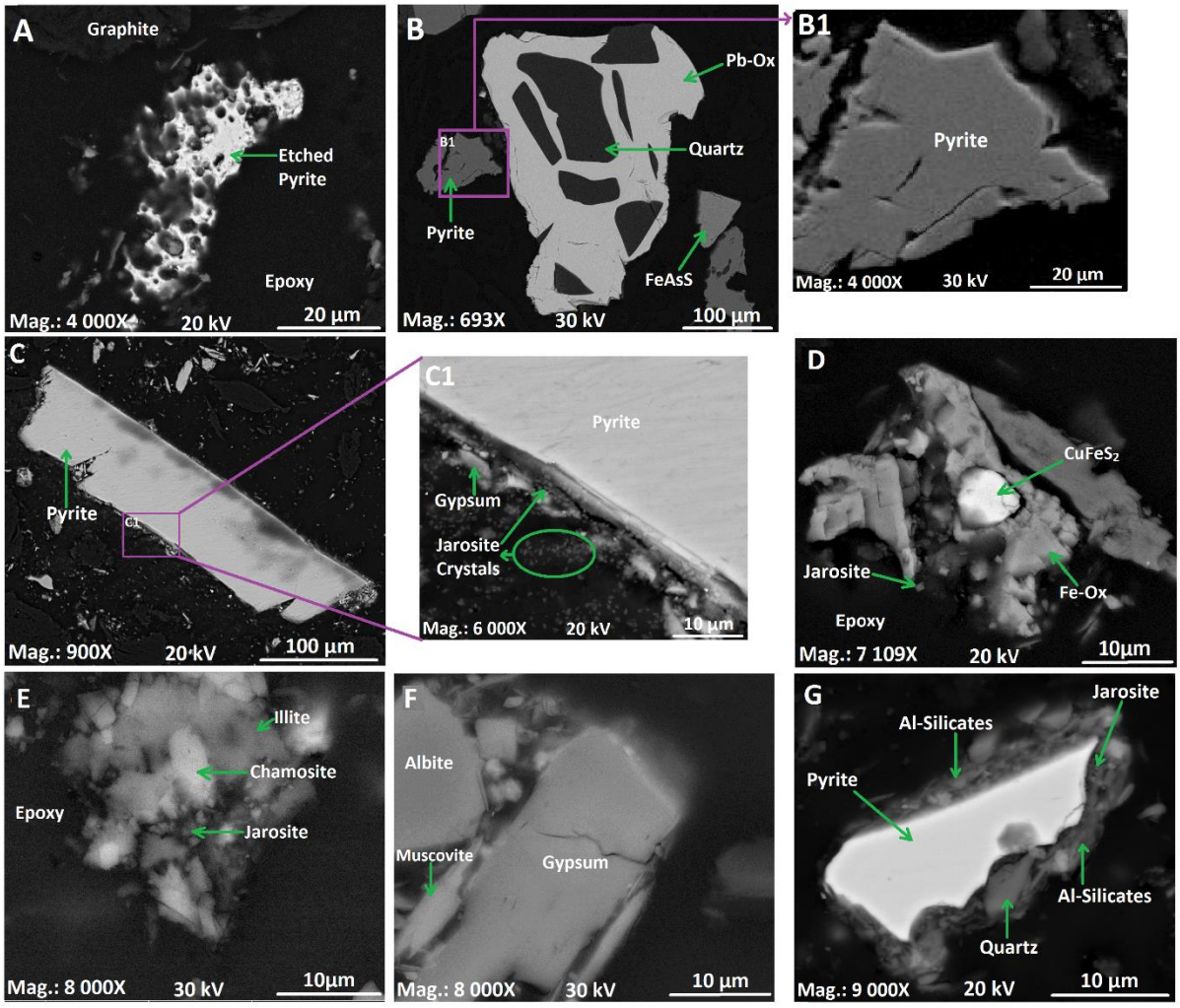

Figure 7. BSE/SEM photomicrographs of the bio-oxidised product yielding lower gold recovery.

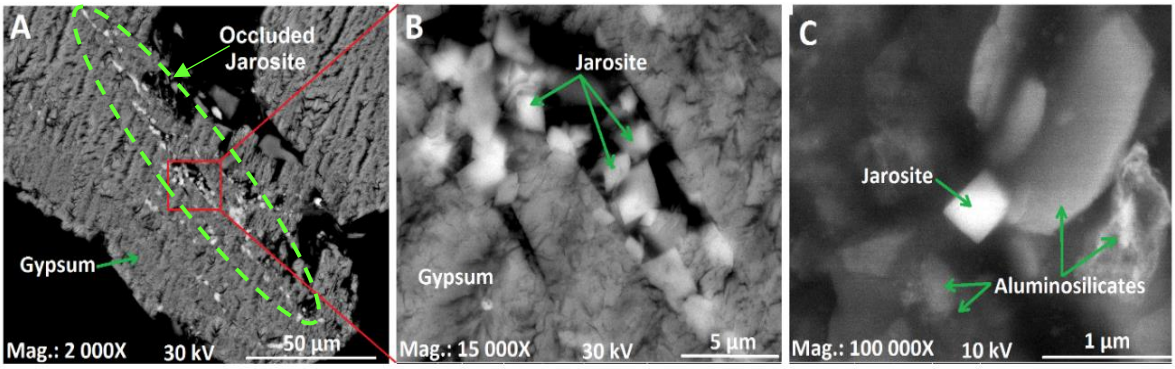

Figure 8. BSE/SEM photomicrographs showing jarosite-gypsum (A and B), and jarosite-aluminosilicate-agglomerate (C) associations in the bio-oxidised product yielding lower gold recovery.

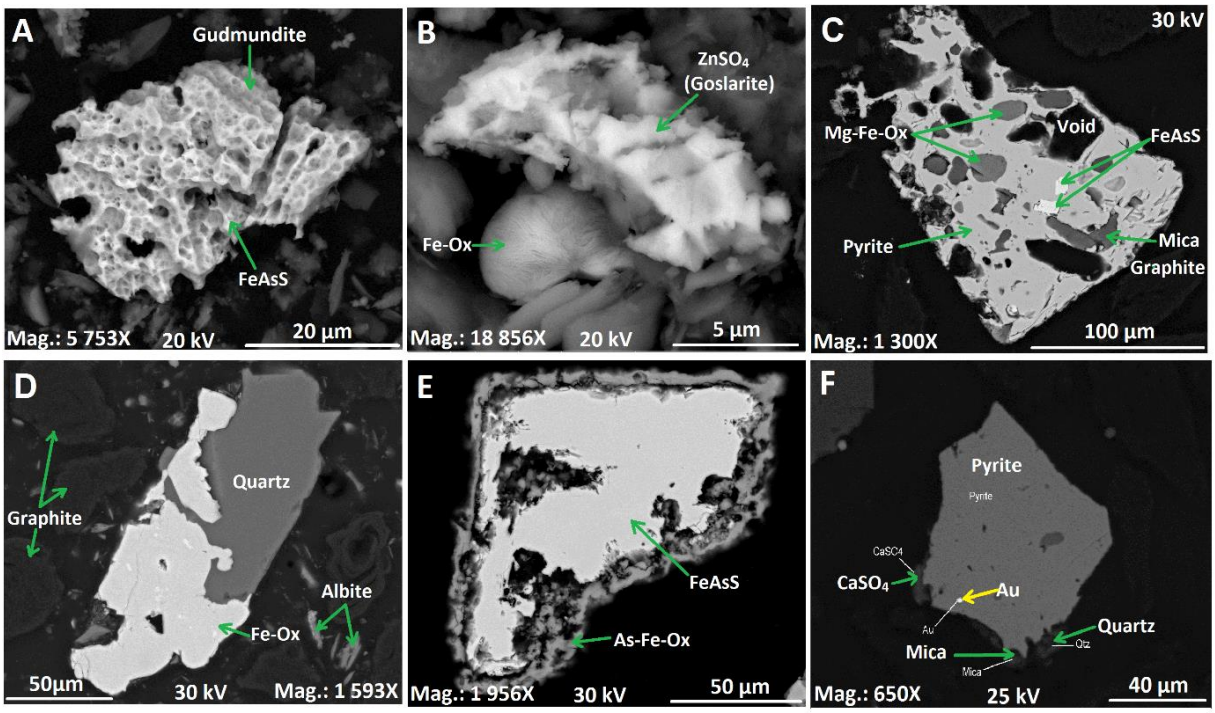

Figure 9 BSE/SEM photomicrographs of the bio-oxidised product yielding higher gold recovery.

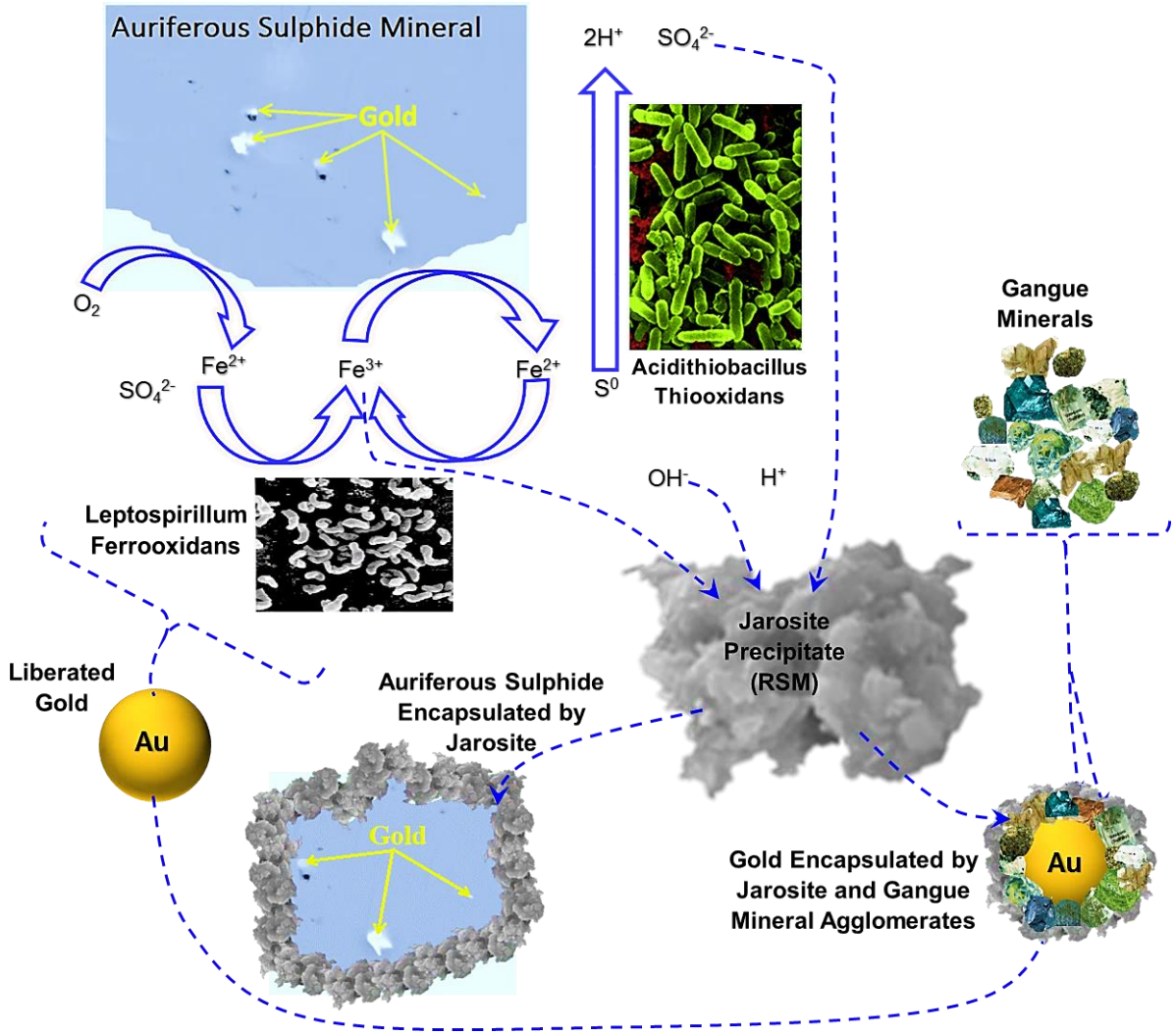

Figure 10 Schematic diagram of the jarosite formation effect on gangue minerals and gold particles in the lower gold yielding bio-oxidised product (BP2).

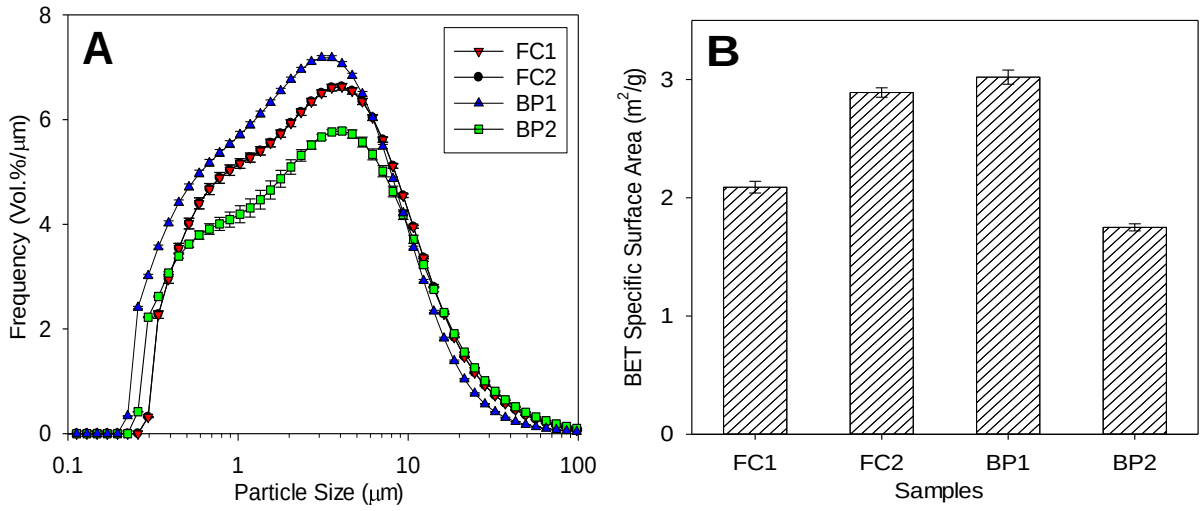

Figure 11 (A) Particle size distribution; and (B) Specific surface area of the flotation concentrates and bio-oxidised products.

List of Tables

Table 1. Classification of gold ores based on the percent of gold recovered after cyanidation (degree of refractoriness), linked with gold liberation and common mineral associations. Modified after Afidenyo (2008).

Table 2 PMA mode of QEMSCAN mineral mass abundance (%) and average grain size (μm) of the investigated flotation concentrates and bio-oxidised products

Table 3 Bulk chemistry of the two comminuted run-of-mine, flotation concentrates, and bio-oxidised product NB: Others include Be, Th, Ta, Sm, Sn, Lu, Gd, Eu, Hf, Ho, Dy, Pt, Pd, Er, Tb, Tl, Tm, U, Cd, and Yb. 95% Confidence Interval.

Table 4 Sulphur speciation in the two comminuted run-of-mine ores, flotation concentrates, and bio-oxidised products.

Table 5 Carbon speciation in the two run-of-mine ores, flotation concentrates, and bio-oxidised products.

Table 6 EDTA extractable metal ions in flotation concentrates and bio-oxidised products

Table 1. Classification of gold ores based on the percent of gold recovered after cyanidation (degree of refractoriness), linked with gold liberation and common mineral associations. Modified after Afidenyo (2008).

Ore Classification		Common Mineral Associations	Au Liberation	Au Recovery
Placer		Platinum, iridosmine, magnetite, pyrite, ilmenite, zircon, garnets, and baryte.	Fully liberated native Au – No comminution required.	100%
Free-milling		Quartz, pyrite, arsenopyrite, feldspar, mica, chlorite, and carbonate minerals.	Unliberated Au – Fully liberated after comminution.	More than 90%
Oxidized		Haematite, magnetite, goethite, limonite, clay minerals	Either liberated or occluded by alteration products.	Variable – Based on association
Refractory	Mildly	Tellurides, complex association with pyrite, arsenopyrite, quartz, copper minerals, galena and carbonaceous material. Degree of refractoriness increases with complexity of Au-gangue association and gangue mineral effect on cyanidation. Sub-microscopic gold in gangue minerals especially arsenopyrite.	Unliberated Au. Partially - fully liberated after ore pre-treatment. Pre-treatment success determines recovery of Au.	80 - 90%
	Moderately			50 - 80%
	Highly			Less than 50%

Table 2 PMA mode of QEMSCAN mineral mass abundance (%) and average grain size (μm) of the investigated flotation concentrates and bio-oxidised products

Mineral Phases	Description	FC1		FC2		BP1		BP2	
		Mineral Mass (%)	Average Grain Size (μm)	Mineral Mass (%)	Average Grain Size (μm)	Mineral Mass (%)	Average Grain Size (μm)	Mineral Mass (%)	Average Grain Size (μm)
Pyrite	FeS_2 associations	36.0	35.1	24.2	13.7	0.7	13.9	1.0	6.4
Arsenopyrite	FeAsS associations	7.5	11.2	5.0	8.6	0.1	6.9	0.1	5.9
Pyrrhotite	FeS and Fe_7S_8 associations	1.1	4.5	0.3	4.6	0.0	2.9	0.1	3.1
Chalcopyrite	$CuFeS_2$ associations	0.0	6.1	0.0	5.8	0.2	4.3	0.3	5.0
Other Sulphides	Chalcocite, digenite, galena, sphalerite, tetrahedrite, and heideite associations	0.2	8.0	0.2	8.1	0.0	3.4	0.1	4.8
Quartz	SiO_2 mineral associations	17.1	16.2	27.3	9.8	35.7	9.1	33.3	10.4
Feldspar	Albite, orthoclase, sanidine and plagioclase associations	4.0	13.2	4.6	8.4	4.9	8.7	5.1	8.8
Kaolinite-Serpentine	Kaolinite and serpentine mineral group	1.6	5.0	2.9	4.4	3.0	3.6	4.1	3.7
Amphibole/Epidote/ Cordierite	Pumpellyite, cummingtonite, clinozoisite, cordierite and ferrohornblende associations	0.5	4.1	0.2	4.7	0.2	4.1	0.1	3.4
Muscovite/Illite/ Biotite	Muscovite, illite, ephesite and biotite associations	20.2	15.3	23.2	8.2	32.8	7.4	32.6	9.1
Pyroxene/Garnet/ Olivine	Almandine, chromite, diopside, greenalite, calico-olivine and bertierine associations	3.1	3.9	2.2	4.5	0.1	3.9	0.1	3.8
Chlorite/Smectite/ Pyrophyllite/Talc	Talc, pyrophyllite, chamosite, minnesotaite and nontronite associations	1.0	4.1	2.6	5.0	3.8	3.9	1.4	3.9
Dolomite/Ankerite	Dolomite and ankerite associations	5.2	14.0	0.8	9.6	0.0	3.7	0.0	5.5
Other Carbonates	Calcite, siderite and malachite associations	0.1	4.6	0.1	4.2	0.1	5.8	0.2	5.2
Apatite	$Ca_5(PO_4)_3$ mineral associations	0.1	7.9	3.8	7.4	0.0	5.5	0.1	6.4
Rutile/Ilmenite	Rutile, leucoxene and ilmenite associations	1.2	7.1	1.4	7.7	2.6	7.2	2.0	6.8
Magnetite/Hematite /Goethite	Fe_3O_4, Fe_2O_3 and FeO(OH) associations	0.5	12.0	0.7	8.1	2.5	6.6	2.2	10.1
Jarosite	Jarosite, natro-, plumbo- and argento-jarosite associations					0.0	2.9	5.5	3.2
Anhydrite	$CaSO_4$ associations					13.1	20.9	11.5	18.6
Others	Stilpnomelane, gersdorffite, stannite, scheelite, corundum and unclassified phases	0.6	4.8	0.5	5.0	0.2	3.3	0.2	3.4

Table 3 Bulk chemistry of the two comminuted run-of-mine, flotation concentrates, and bio-oxidised products. NB: Others include Be, Th, Ta, Sm, Sn, Lu, Gd, Eu, Hf, Ho, Dy, Pt, Pd, Er, Tb, Tl, Tm, U, Cd, and Yb. 95% Confidence Interval.

Elements	Unit	ROM1	ROM2	FC1	FC2	BP1	BP2
Fe	%	7.7	13.3	19.2	14.2	5.1	5.8
Si		34.2	28.8	15.3	21.4	28.1	27.5
Al		10.4	9.9	5.9	7.7	10.5	9.9
Ti		0.3	0.7	0.7	0.7	1.1	1.1
Ca		1.8	1.6	1.3	0.8	3.9	3.7
Total S		1.4	1.0	18.1	10.7	3.6	5.1
Mg		1.8	3.4	1.0	0.9	0.4	0.5
K		2.3	0.9	1.2	1.6	2.1	2.0
As		0.3	0.1	2.6	2.0	0.2	0.4
Na		1.6	1.1	0.8	1.0	1.3	1.6
Mn	ppt	1.1	2.3	0.5	0.6	0.0	0.2
P		0.8	0.9	0.4	6.8	0.7	1.0
Zn		0.1	0.3	0.5	0.3	0.1	0.1
Pb		0.0	0.1	0.2	0.0	0.0	0.0
Cu		0.1	0.1	0.7	0.8	0.2	0.4
Ba		0.7	0.4	0.4	0.6	0.6	0.7
V		0.1	0.4	0.2	0.1	0.2	0.2
Cr		0.1	0.1	0.1	0.1	0.1	0.2
Cl		0.0	0.0	0.0	0.0	0.0	0.0
Ni		0.1	0.1	0.5	0.3	0.0	0.0
Co		0.0	0.1	0.3	0.1	0.0	0.0
Sr		0.4	0.3	0.3	0.1	0.4	0.4
Zr		0.1	0.0	0.3	0.3	0.2	0.2
Ag	ppm	0.3	0.3	1.8	4.4	3.8	3.7
Au		2.8	1.3	27.5	16.9	38.2	23.0
Ce		52.2	40.0	69.3	80.1	125.2	131.2
Cs		14.6	8.0	9.0	12.2	14.9	14.7
Ga		25.2	26.5	12.5	18.8	28.0	27.0
La		26.9	18.8	32.8	39.3	65.3	65.0
Mo		2.7	5.3	7.7	13.3	9.5	11.0
Nb		3.3	7.2	8.4	11.5	17.3	17.9
Nd		26.4	21.5	37.7	41.5	62.8	64.8
Pr		6.5	5.3	8.7	10.2	16.0	16.4
Rb		104.8	50.9	58.1	80.5	103.7	105.2
Sb		33.5	26.5	207.6	208.6	314.8	350.7
Sc		27.8	43.1	14.5	18.8	25.6	23.3
Te		0.0	0.0	1.5	1.3	1.2	1.0
W		15.7	25.2	53.3	68.7	107.9	105.5
Y		12.9	36.8	38.4	45.7	73.7	64.0
Others		25.0	46.7	48.6	63.2	89.3	83.9
LOI*	%	9.2	9.7	22.0	19.2	16.9	17.2

***LOI – Loss on ignition**

Table 4 Sulphur speciation in the two comminuted run-of-mine ores, flotation concentrates, and bio-oxidised products.

Samples	Sulphate-Sulphur (wt.%)	Sulphide-Sulphur (wt.%)	Elemental Sulphur (wt.%)	Total Sulphur (wt.%)
ROM1	0.03 ± 0.01	1.33 ± 0.13	< 0.05	1.36 ± 0.14
ROM2	0.07 ± 0.01	0.96 ± 0.10	< 0.05	1.03 ± 0.12
FC1	0.17 ± 0.02	17.93 ± 1.79	< 0.05	18.10 ± 1.81
FC2	0.11 ± 0.01	10.54 ± 1.05	< 0.05	10.65 ± 1.07
BP1	2.92 ± 0.29	0.63 ± 0.06	< 0.05	3.55 ± 0.36
BP2	4.10 ± 0.41	0.99 ± 0.10	< 0.05	5.09 ± 0.51

Table 5 Carbon speciation in the two run-of-mine ores, flotation concentrates, and bio-oxidised products.

Samples	Graphitic Carbon (wt.%)	Non-Carbonate Carbon (wt.%)	Carbonate Carbon (wt.%)	Total Carbon (wt.%)	PEC (g/t)	PRV [(g/t)/wt.%]
ROM1	1.10 ± 0.11	1.49 ± 0.15	1.30 ± 0.13	2.79 ± 0.28		
ROM2	0.30 ± 0.03	0.46 ± 0.05	1.10 ± 0.11	1.56 ± 0.16		
FC1	4.40 ± 0.44	5.04 ± 0.50	1.05 ± 0.10	6.30 ± 0.63		
FC2	4.20 ± 0.42	4.60 ± 0.46	0.14 ± 0.01	4.74 ± 0.47		
BP1	4.20 ± 0.42	5.70 ± 0.57	0.20 ± 0.02	5.90 ± 0.59	40.84 ± 2.04	7.16 ± 0.36
BP2	2.30 ± 0.23	4.20 ± 0.42	0.30 ± 0.03	4.50 ± 0.45	21.80 ± 1.09	5.19 ± 0.26

Table 6 EDTA extractable metal ions in flotation concentrates and bio-oxidised products.

Samples	As_{EDTA}/As_T (%)	Ca_{EDTA}/Ca_T (%)	Cu_{EDTA}/Cu_T (%)	Fe_{EDTA}/Fe_T (%)	K_{EDTA}/K_T (%)	S_{EDTA}/S_T (%)
FC1	0.10 ± 0.01	6.70 ± 0.67	1.20 ± 0.12	0.10 ± 0.01	2.40 ± 0.24	0.50 ± 0.05
FC2	0.20 ± 0.02	0.10 ± 0.01	0.50 ± 0.05	0.20 ± 0.02	2.70 ± 0.27	0.10 ± 0.01
BP1	21.20 ± 2.12	7.00 ± 0.70	0.80 ± 0.08	2.80 ± 0.28	2.20 ± 0.22	0.40 ± 0.04
BP2	49.90 ± 4.99	15.80 ± 1.58	2.00 ± 0.20	15.30 ± 1.53	2.90 ± 0.29	5.60 ± 0.56